Dry Sliding Wear Behaviour of T6-Aluminium Alloy Composites Compared with Existing Aircraft Brake Pads

P. Ashwath[1] · M. Anthony Xavior[1]

Abstract

Current research investigates the effect of casehardening, plasma nitriding and T6 heat treatment condition on the dry sliding behaviour of microwave-assisted T6-AA2900-α-Al$_2$O$_3$ composite material against aircraft disc material. Composite samples without post-treatment were also considered for the evaluation. Experiments were carried out with a pin-on-disc wear tester at maximum brake operation temperature of 450 °C. The results show that formation of Al$_4$C$_3$ and AlN on the surface and near subsurface influences the coefficient of friction and the specific wear rate regimes close to aircraft brake operating parameters. The developed composite material featuring homogeneously dispersed α-Al$_2$O$_3$, homogeneously nucleated Al$_4$C$_3$ exhibits a better behaviour, as compared to surface formed AlN. The results were obtained comparing explicit characteristics (i.e. braking COF-wear and temperature effects) of the surface modification on T6-composite under the aircraft braking conditions. Counter disc characterisation was also carried out to understand the impact of the surface modification, temperature effects and microwave T6 condition.

1 Introduction

Current research area focussing on aircraft brake pads for Boeing is associated with modern convention aiming at reducing the percentage of copper present in the brake pads. Certainly, copper percentage reduction close to 0.5 wt% is aimed by the U.S. Legislation before 2025 [1]. However, copper poses vital properties, such as good thermal conductivity and the capability to alleviate the coefficient of friction, which is favourable to the aircraft brake pad efficiency [2, 3]. Hence, while addressing the copper wt% reduction, prospective alternatives which can fulfil the needs are to be studied. Existing materials used to produce aircraft brake pads are made of various constituents with Fe as the major matrix and graphite as the added constituent [4]. The composite materials used for friction application are distinguished based on their major function as: reinforcements, binders, fillers and friction additives [5, 6]. The additives used in composite frictional materials can be differentiated

into two major types: lubricant and abrasive. Lubrication additives are used to stabilize frictional coefficient of the developed composite and assist regulating the formation of the friction cover, as a result of contributing to reduction in total wear loss. A steady sliding characteristic, i.e. steady state of the frictional coefficient, is necessary for superior aircraft brake performance. In this direction, various ceramic reinforcements and alloying elements as constituents are commonly used in the aluminium alloy composite aircraft brake pad formulations [7]. There are various research works validating the effect of ceramic addition to the aluminium matrix for their tribological performance in friction application, i.e. Al$_2$O$_3$ and SiC, but very few research works are noticed which are addressing the effect of bulk treating and surface modification on the aircraft braking scenarios. In general, aluminium alloy metal matrix composite (AAMMC) offers superior resistance to wear and surface seizure as compared to the monolithic aluminium alloy irrespective of operational load and sliding speed. This phenomenon is principally appropriate to the fact that the ceramic dispersoids make the aluminium alloy plastically embarrassed and enhance the high-temperature potency of the virgin alloy [8]. Inadequate attempts have been carried out to observe the influence of T6 condition on the dry

✉ M. Anthony Xavior
  manthonyxavior@vit.ac.in

1 School of Mechanical Engineering, Vellore Institute
   of Technology, Vellore 632014, India

sliding wear performance of aluminium composites. Several research works have reported that overaged aluminium composites demonstrated superior wear resistance while comparing the composites that are under aged. According to these facts, this disparity is endorsed to the respite of tensile stresses induced in the matrix particle and compressive stress forced onto the added ceramic materials during T6 conditions [9].

Overall stress relaxation is observed to be high in the over-aged composites which leads to fewer fracture of reinforcement and leads to development of additional steady shielding layer above the surface of the composite [9–11]. In view of the aircraft brake friction application, the counter disc part, i.e. the rotors surface damage, should be considered while developing an alternate lightweight friction material added with ceramic constituents. Most of the ceramic constituent such as carbides and nitrides are highly abrasive in nature which counters the disc parts during operational conditions [12]. Al_2O_3 by its nature has excellent compressive load bearing capacity and less abrasive in nature because of which it found its place as a successful reinforcing agent for aircraft brake friction application [13]. The reinforcement material should be less abrasive in nature and should have a great load bearing capacity in order to qualify for adding with aluminium matrix for developing the aircraft brake friction material. Microwave-assisted bulk treatment like T6 treatment and case hardening on the composite improves the surface tribological properties like wear resistance, total wear loss and good strength behaviour [14]. For aluminium alloys, the formation of AlN layer can be achieved by plasma nitriding process. In general, plasma nitriding is a proven process to enhance the poor tribological properties of aluminium composites and its alloys [15]. Thermal and chemical stability of the composite surfaces can be achieved by surface modification and bulk treating techniques [16]. Very few research works addressed the application of post-processing of the lightweight alloys and their composites in an aircraft brake pads application. Current research focus on developing a composite with major matrix constituent as aluminium alloy 2900 reinforced with 6 wt% alumina (α-Al_2O_3). Literature revealed that the brake pads and brake disc materials were fabricated mainly using copper-based and ferrous-based materials. Experimental studies on using lightweight materials combinations for the applications are not available in the open literature. Investigations on AAMMCs brake friction materials against a cast iron disc in a pin-on-disc system are reported elsewhere, whereas the behaviour of aluminium alloy to aluminium alloy composites brake friction studies was not investigated. The fabricated composite is post-processed with microwave-assisted T6 standard heat treatment method as per ASTM standard followed for 2024-T6. Continuing the post-processing, the T6-heat-treated composite surfaces are surface processed with microwave case hardening and plasma nitriding techniques. The tribological validations of the novel composites were reasonably investigated on a high temperature-assisted pin-on-disc wear tester (PoD). Eventually, this testing grid cannot duplicate actual brake operation scenarios, for which precise types of testing equipment, e.g. shear tester and brake inertia dynamometer, are available. However, PoD can relatively examine the developed composite in a well-timed approach and impact of test conditions have on the composites performances. Tests were performed at maximum brake operating temperature of 450 °C. High-resolution SEM observations, X-ray spectral analyses, surface roughness validation after the wear test by probe method and atomic force microscopy methods and scratch test were performed on the composite surface layer which is post-processed, to attain a concrete understanding of the aircraft brake pads friction material replacement.

2 Materials and Methods

2.1 Materials

Current research work focuses on developing and validating aluminium alloy composites fabricated by powder metallurgy route and synthesized by microwave processing technique. Matrix material used for fabricating composites is aluminium alloy 2900 (AA2900), and the reinforcement material used is α-Al_2O_3. α-Al_2O_3 was procured from Carborundum Universal Limited, Kerala, India. The metal powder AA 2900 was purchased from AMPAL Inc. USA. Handheld X-ray florescence analyser has been used for confirming the alloying elements, and their percentage in AA 2900 matrix is shown in Table 1.

The added constituents can be classified according to standard categories such as: matrix metal (aluminium alloy); reinforcement additives (aluminium oxideα-Al_2O_3); precipitates formed (Al_4C_3, Al_2Cu and Al_2CuMg). Figure 1 shows the high-resolution scanning electron microscope (HRSEM) micrograph and energy-dispersive X-ray analysis (EDX), in which the composite is labelled with the constituents present on the surface. The red circle marked in the Fig. 1 indicates the dispersed α-Al2O3 in the aluminium matrix.

Table 1 Elemental composition of AA 2900 as received from Ampal Inc. USA

Elements	Al	Cu	Mg	Si	Fe	Sn
Wt%	94.22%	3.25%	1.47%	0.30%	0.09%	0.67%

Additionally, the dark patches indicated by the arrow heads represent the formed Al_2Cu and Al_2CuMg precipitates that are confirmed by the EDAX data with copper and magnesium peaks as shown in Fig. 1.

Composites fabricated by powder metallurgy route were subjected to two different processing techniques followed by microwave-assisted T6 heat treatment methods. In Fig. 2 the HRSEM micrographs with the composite samples post-processed with microwave case hardening and the composite samples surface processed with plasma nitriding process are shown. HRSEM was used to determine the cross-sectional area of the added α-Al_2O_3. Table 2 shows the average

Fig. 1 HRSEM micrograph of the composite processed by microwave T6 treatment showing its constituents
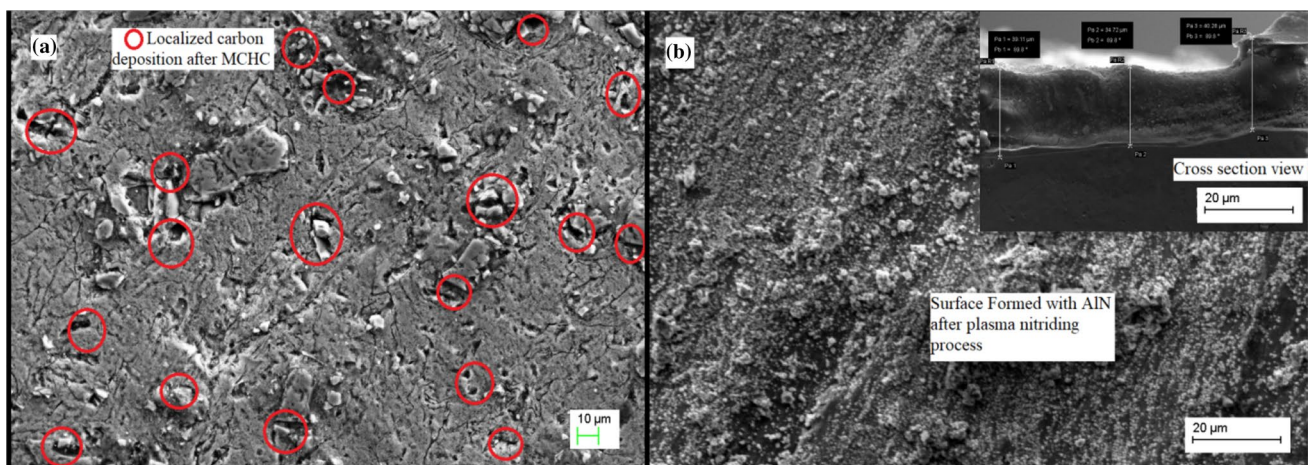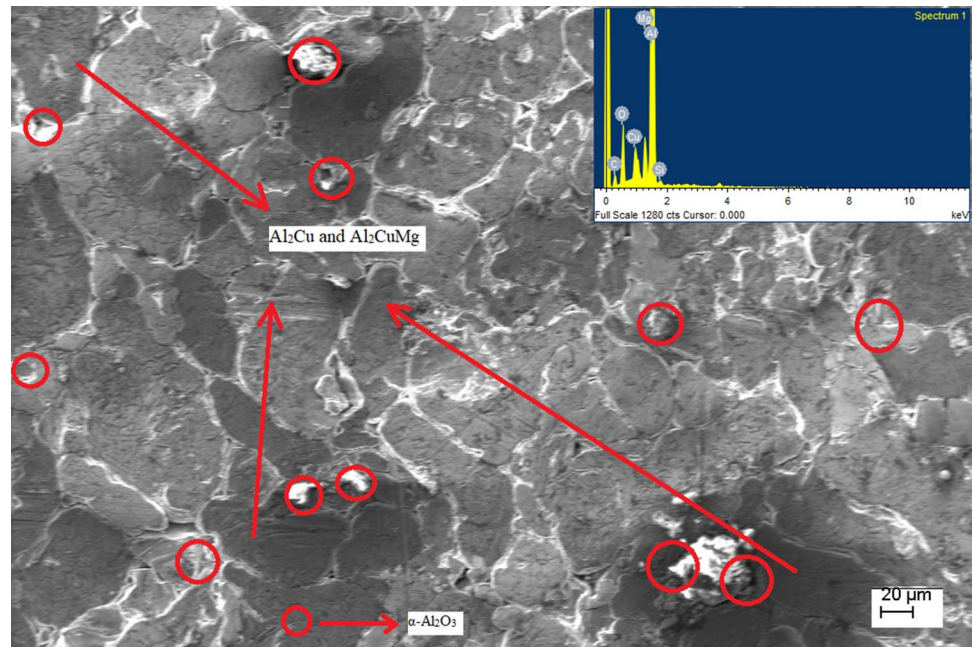

Fig. 2 HRSEM micrographs of the T6 heat-treated composite a T6-CH and b T6-PN with average thickness of AlN 40 µm after 20 h

Table 2 Average area and diameter of α-Al_2O_3 particles in T6, T6-CH and T6-PN composites

Area	A1 (µm)^2	A2 (µm)^2	A3 (µm)^2	A4 (µm)^2	A5 (µm)^2	Avg Area A_{avg} (µm)^2	d (µm)
T6	452	491	506	460	523	486	12
T6-CH	1134	1182	1206	1158	1219	1180	19
T6-PN	707	794	725	754	716	739	15

cross-sectional area of the alumina particles observed and the computed average diameter (d) of the particles for each type of material. The matrix material AA 2900 and α-Al$_2$O$_3$ used were of particle size range 10–20 μm.

The accuracy of digital weighing balance was calibrated around 0.001 g. To remove moisture from the weighed powder mixture, the mixture is loaded to a hot air oven of capacity 400 °C for 60 min. Ball milling was performed for 30 min and at 200 rpm as the objective is to achieve homogeneous mixing. Ball-to-powder ratio of 10:1 was maintained during ball milling. Hydraulic press of capacity 500 tons was used for uniaxial pressing, where the samples are compacted at 450 MPa with 12 min of holding time. The temperature at which microwave sintering performed was 495 °C at 50 °C heating rate. The maximum operation capacity of the microwave furnace is around 1000 °C at 10 KW maximum powers with 2.45 GHz of magnetron and dwell temperature accuracy of 1 °C.

The sintered composites are further solution treated (T6 condition) and quenched in a cold water bath and further artificially aged at 190 °C for 6 h in a microwave oven of maximum capacity 400 °C. The type of surface modification used on the T6 heat-treated composite samples is named as T6-CH (microwave case hardened composites) and T6-PN (plasma nitrided composites). Pack carburizing of T6 treated composites is performed in a sealer crucible filled with pulverized charcoal and barium carbonate mixture. Solution treatment for microwave carburizing on T6-composite was performed at 500 °C for duration of 6 h. For surface processing on T6-composite plasma nitriding technique is used for 20 h of duration. During the process, parameter like vacuum pressure of 3×10^{-3} Pa with 200 sccm (standard cubic centimetre per minute) was followed. Plasma nitriding process was carried out at 500 °C. All tribological test samples were prepared by cutting the bulk samples using wire electric discharge machine.

A fine micro-hole of diameter 2.5 mm was drilled at the centre of the sample to fit the thermal transducer with sensing capacity of 600 °C. In this way, square-shaped composite pins with a breadth, width of 5×5 mm and a height of 45 mm were prepared. The samples were dried after cutting at 100 °C in a vacuum oven for 2 h. The density of the fabricated microwave-assisted T6 composite specimens was calculated by Archimedes principle and found to be 2.57 ± 0.08 g/cm^3 and comparatively the pure alloy AA 2900 had a density value of 2.60 ± 0.06 g/cm^3. Discs made of pearlitic grey cast iron with a diameter of 80 mm and 10 mm in height, with the hardness of 45 HRC, were used as counterpart for the tribological trails.

2.2 Experimental Procedure

The friction and wear validation of the T6-CH and T6-PN specimens were initially characterized at operational temperature (maximum of 450 °C) of the aircraft brake pads. The Ducom TR 201LE tribometer used for the experiments, equipped with a pin heating module with maximum temperature output of 600 °C, was manufactured by Ducom Instruments, Bangalore, India. A closed-loop feedback circuit arrangement held the pin temperature stable throughout the experiment, using a probe type high-temperature transducer inserted inside the pin.

The sliding velocity was 8 m/s and brake operational pressure of 4 MPa was achieved in PoD grid by loading 100 N forces in all trails. These operational conditions, followed in earlier actual brake operational parameters, are anticipated to attain actual braking condition in PoD grid [17]. The interval of the each trail is planned for the total braking or stopping distance calculated from the total runway landing distance. Figure 3 shows the schematic diagram of the braking distances for the runway. Current brake pads life is measured in terms of 120 individual landings of service period or 1.5 mm of total pads wear with 0.35 of constant COF. There are three distances to be noticed in the aircraft braking scenarios. Those are calculated landing distance, required landing distance with safety factor and landing distance available. The landing distance available for the aircraft to land is 250 m. The experimental trails are

Fig. 3 Landing schematic drawing of a runway (courtesy: Text book, Aircraft Systems by Allan Seabridge)
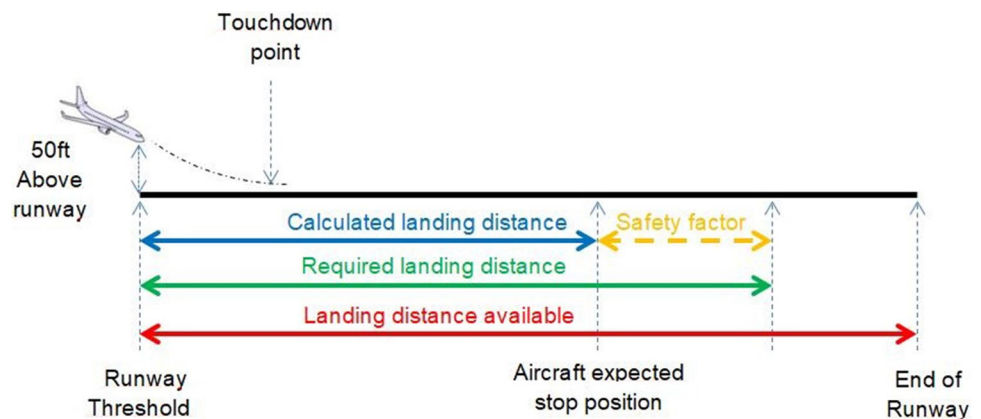
planned in two different methods: one is continuous wear and the other for the stopping distance. The continuous wear test was performed for total landings during their service period which is 120 landings. The total time for the test is calculated from the circumferential formula of the circle $2 * \pi * r$, where r is the track radius 35 mm. The stopping distance of the aircraft is calculated based on considering the required landing distance, and it is estimated as 250 m approximately. The stopping distance is calculated from the formula given in Equation – 1:

$$d = \frac{v^2}{2 \times \mu \times g} \qquad (1)$$

where d = stopping distance (m), v = velocity (m/s), μ = coefficient of friction, g = acceleration due to gravity (9.8 m/s^2).

Calculated time for each trail of continuous wear for the total service period is around 6000 s and 30,000 m. To perform the single stopping distance validation using the processed pins, the same input conditions are used and the power supply to the rotating disc was stopped so that pin in contact acted with pressure of 4 MPa tries to stop the disc which gives the stopping time and distance that are recorded with a stop watch and a tachometer.

Four individual tests were performed for the specimens to ensure the accuracy of the experiments conducted, and the presented data for coefficient of friction and total wear loss are the average of 4 observations. Composite specimens are removed from the pin heating module after each test and recorded for the surface roughness values, and the counter disc part is removed and evaluated for the surface roughness validation. The wear rate was validated by weighing the composite pin before and after the experiment with a digital balance having an accuracy of 10^{-4}gms. The coefficient of friction was constantly monitored and recorded using a load cell. The specific wear coefficient (K_c) of the composite specimens tested at elevated temperatures is calculated by formula given in Eq. 2, 3 and 4 [23, 24]: specific wear coefficient is a function of the sliding distance, which is the total number of landings multiplied by the distance for each landing. K_C is calculated in the steady-state regime of the total wear recorded from the continuous wear test for 30,000 m.

$$K_C = \frac{3Hd(1 - f_V)m_A}{Pg_1 f_V L_s} \left[1 - \exp\left(\frac{-g_3 f_V L_s}{d(1 - f_V)} \right) \right] \qquad (2)$$

$$g_1 = \frac{Hm_A}{P} \qquad (3)$$

$$g_3 = \frac{d(1 - f_V)}{f_V} \frac{(\ln m_A - \ln m_B)}{L_s} \qquad (4)$$

$$L_s = L_q - L_t \quad V_s = V_q - V_t \qquad (5)$$

where H is hardness of composite pin, d is the average size of α-Al$_2$O$_3$, P is the applied load, f_V is the α-Al$_2$O$_3$ volume fraction, L is the total landing distance opted for continuous wear test, g_1 and g_3 are the experimental constants for wear test calculated from Eqs. 3 and 4. From Fig. 6 to calculate g_1 and g_3, the gradients of the volumetric composite pin material loss (V_C) be m_A at $L = 0$, m_B at $L = L_t$ which is the beginning of the steady-state wear. Total sliding distance at the steady-state L_s is used to calculate the K_C in the current research which is obtained by Eq. 5, where L_q is the total sliding distance including sliding distance in transient mode L_t and sliding distance at steady-state mode L_s. V_q is the total volume loss at transient mode V_t and at steady-state mode V_s. The tested surface of the composite pins was observed with Quanta 200 FEG high-resolution scanning electron microscope (HRSEM), equipped with energy-dispersive X-ray analysis (EDX). The pins were observed both in planner and sectional directions. The surface of the pins were cut and embossed in an epoxy resin medium, cured into solid state in oven and then tested for the surface roughness validation. Counter disc part was also validated after each test by optical inverted microscope (Dewinter Model-Dmi Premium), and surface roughness was measured on the wear track to understand the effect of temperature and the surface processing on the composite. Wear chip morphology was also carried out for the composite pin to understand the surface behaviour after the continuous wear and wear test for the stopping distance.

3 Results

3.1 Friction and Wear Behaviour

Surface roughness of the fabricated AAMMC for wear testing on a pin on disc setup needs to be studied. Surface roughness validation is done using stylus-based Mitutoyo Marsurf XR 20 with R probe surface roughness tester. Range of measuring up to 150 mm in depth and double arm length with a range of 500 µm with GD 120 drive motor are equipped to ensure accurate measurements. The surface of the composite after the testing was also measured using the same equipment in the horizontal direction with a standard 4 mm measuring span. The surface average roughness (R_a), root mean square surface roughness (R_q) and mean depth of deepest valley (R_v) are measured with keeping the cut-off span distance of (λc) 3 mm (if $2 < R_a < 10$ µm, $10 < R_z < 60$ µm). Table 3 shows R_V value of 3.439 µm was recorded for the T6-CH. This phenomenon is in good agreement with the process outcomes [18]. But in case of T6-PN,

Table 3 Surface roughness of the T6-composite prepared for wear test

Sample (AA 2900 – 6 wt% Al$_2$O$_3$)	Ra (µm)	Rq (µm)	Rv (µm)
T6 treated	0.870	1.229	2.463
Case hardened	1.354	2.006	3.439
Nitrided	1.195	1.695	2.732

Ra average, Rq root mean square, Rv the depth of the deepest valley from the mean

the sample surface exhibited average surface roughness values close to plain T6 treated ones [19, 20].

Scratch test was performed on the samples processed with CH and PN using a Ducom scratch tester TR 101 with maximum load capacity (i.e. normal and tangential) of 200 N, maximum stroke length of 50 mm and maximum scratch speed of 10 mm/sec. surface roughness profiles are recorded

using the methods mentioned in earlier sections. Scratch testing was performed at 100 N loads for 15 mm length.

Figure 4 c and d clearly indicates that the width of the scratch is considerably decreasing on the T6-CH and T6-PN samples. Figure 4 a exhibits wider scratch because of the ductile nature seen in the pure alloy which receives the load completely to form a deep and wider scratch. This behaviour is seen in the pure alloy as there is high dislocation density seen in the matrix metal when not reinforced (i.e. 400 µm wide). To overcome such surface failure the matrix material is reinforced with 6 wt% α-Al$_2$O$_3$ and the resulting composite is subjected to T6 heat treatment which exhibited some resistance to the induced scratches as shown in Fig. 4 b and b (i.e. 290 µm wide). Such improvement in surface scratch resistance is obtained in the T6-composite samples because of the harder ceramic phase and precipitates that are present on the surface which offer resistance to the load acting on the surface. In addition to the precipitate formation, the
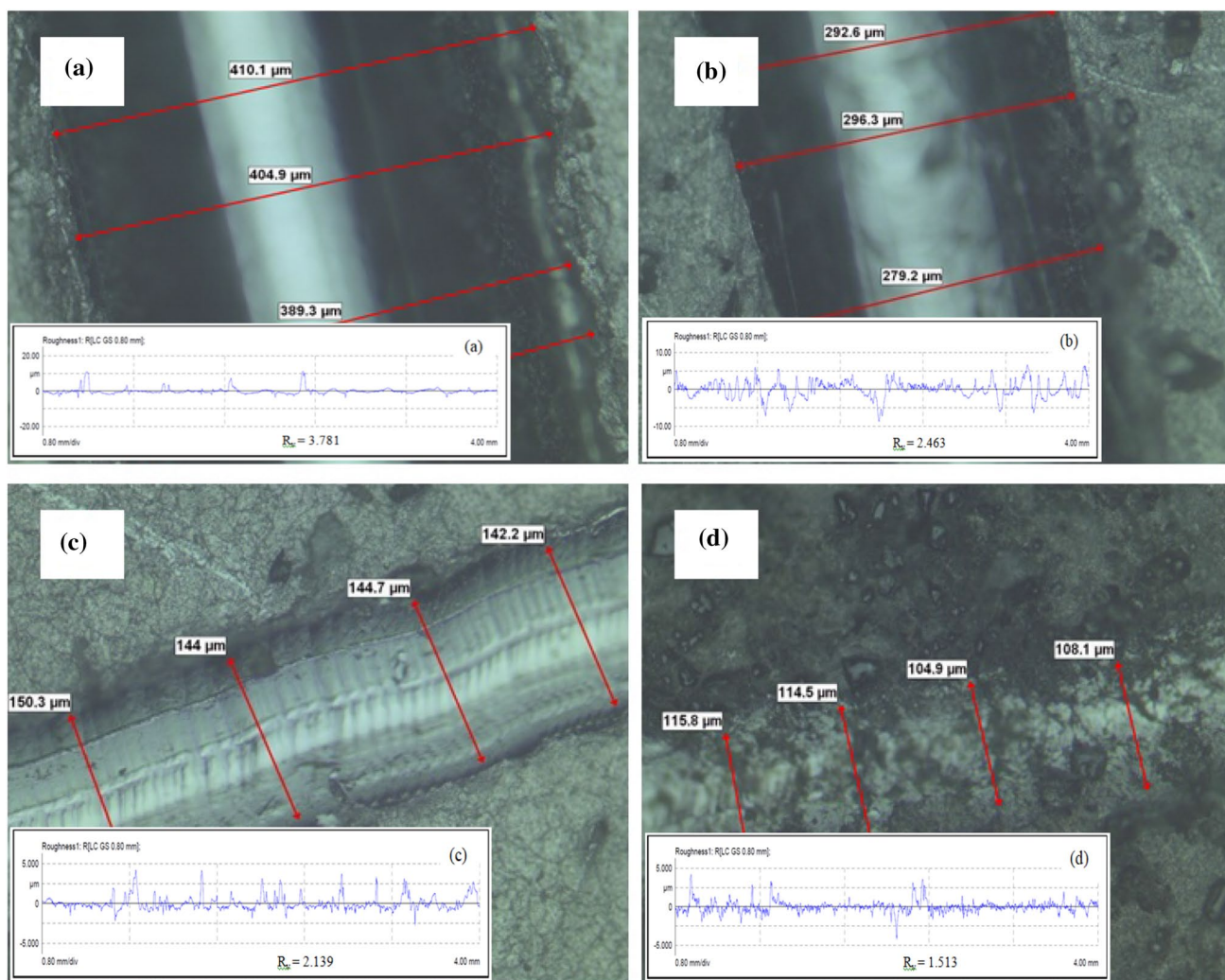

Fig. 4 Scratch test and surface roughness profiles of processed T6 composite **a** pure alloy, **b** T6-composite, **c** T6-CH and **d** T6-PN

Springer

bonding strength between the matrix-reinforcement-precipitate is more important to achieve good scratch resistance surface which was achieved by microwave-assisted T6 process on the composite fabricated.

Figure 5 shows the progression of frictional coefficient (μ) recorded from the PoD setup at maximum brake pads operating temperature of 450 °C (i.e. calculated for total number of landing counts). Figure 5 infers that the COF at the beginning of the continuous mode exhibited a peak and got stabilized in the prolonged testing regime. This kind of behaviour is because of the higher surface roughness that was recorded for T6-CH samples which exhibits higher frictional force at the contact interface that led to higher COF. After prolonged exposure to 450 °C, Sn content in the matrix alloy acted as a solid lubricant at the interface reducing the COF eventually the frictional force at the interface. This phenomenon is evident from the EDX data recorded after the process on the contact composite pin surface and the wear debris showing the Sn content as tabulated in Table 5. As Sn melting point is 231.9 °C, it tends to melt down and oozes out to the interface contact composite surface tested at 450 °C acting as a lubricating film reducing the frictional force and COF eventually. But T6-PN samples exhibited clean and steady COF without any major fluctuation in the values of frictional force. This confirms that AlN formed on the T6 composite surface is firmly bonded with the substrate and exhibits good frictional behaviour. Microwave T6 treated samples also exhibited clean and steady COF without any fluctuation throughout the testing duration [21, 22]. This phenomenon is in good agreement with the earlier results research, density and hardness discussion as

microwave-assisted heat treatment of the AAMMC has provided good interparticulate bonding which made the composite surface firm and uniformly nucleated Al_2Cu [21, 22]. Homogenously dispersed α-Al_2O_3 and uniformly nucleated Al_2Cu exhibited consistent COF [22].

From Fig. 6 it is very clear that highest wear in microns was recorded for samples that are T6 processed. Lowest wear was recorded for T6-CH samples. T6-PN samples exhibited wear performance close to T6-CH samples. It is observed from the wear data that after 2100s of total testing time the AlN layer has completely worn out for 100 N loads at 450 °C and recording total wear of 500 μm (± 15 μm).

The progression of COF at steady state ($μ_{SS}$) and the calculated specific wear coefficient of the composite at steady state (K_C) are presented in Table 4 and displayed in Fig. 7 for good understanding. The composite sample treated for microwave-assisted T6 treatment displays lowest specific wear coefficient (K_C) and frictional coefficient ($μ_{SS}$) at steady state. Composite surface which is treated with microwave-assisted case hardening method displays the highest K_C and $μ_{SS}$. Moreover, not much scatters in the standard deviation bars are observed from Fig. 7. T6-PN composite pins display the slightly higher and closer K_C and $μ_{SS}$ when compared with the T6-composite.

3.2 Analysis of Composite Surfaces and Counter Disc Part Tested for continuous and Stopping Distance Wear Test

Figure 8 exhibits the HRSEM images of the composite samples tested with continuous wear. From Fig. 8, it is inferred
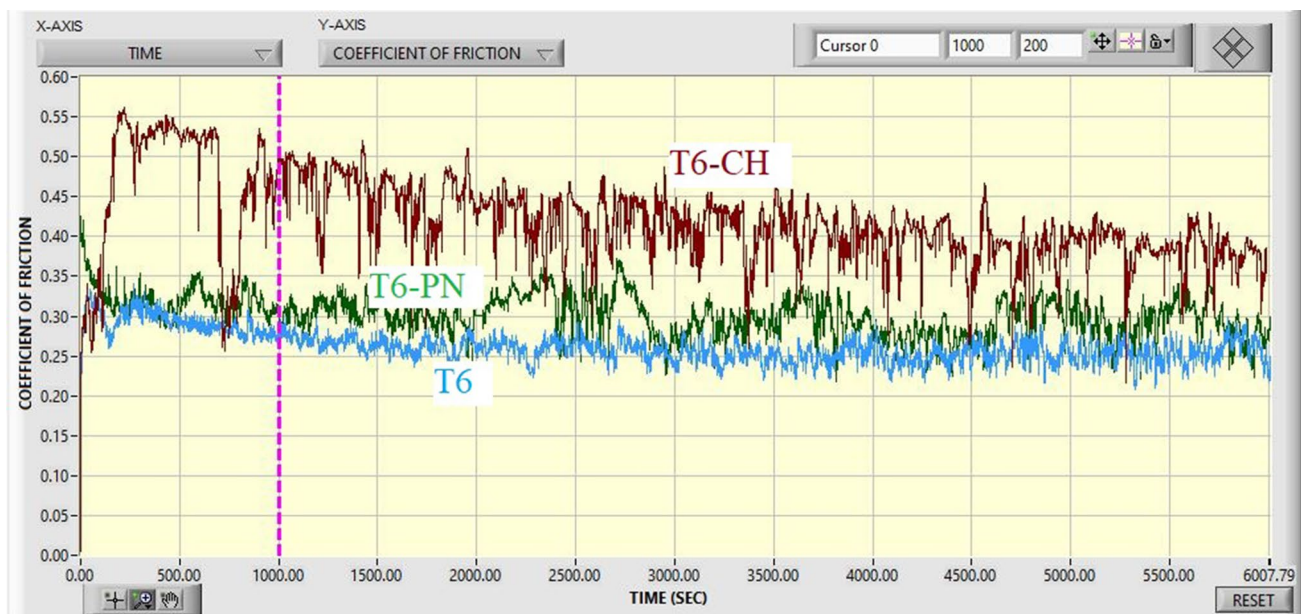

Fig. 5 Coefficient of friction recorded for AAMMC for continues wear testing mode
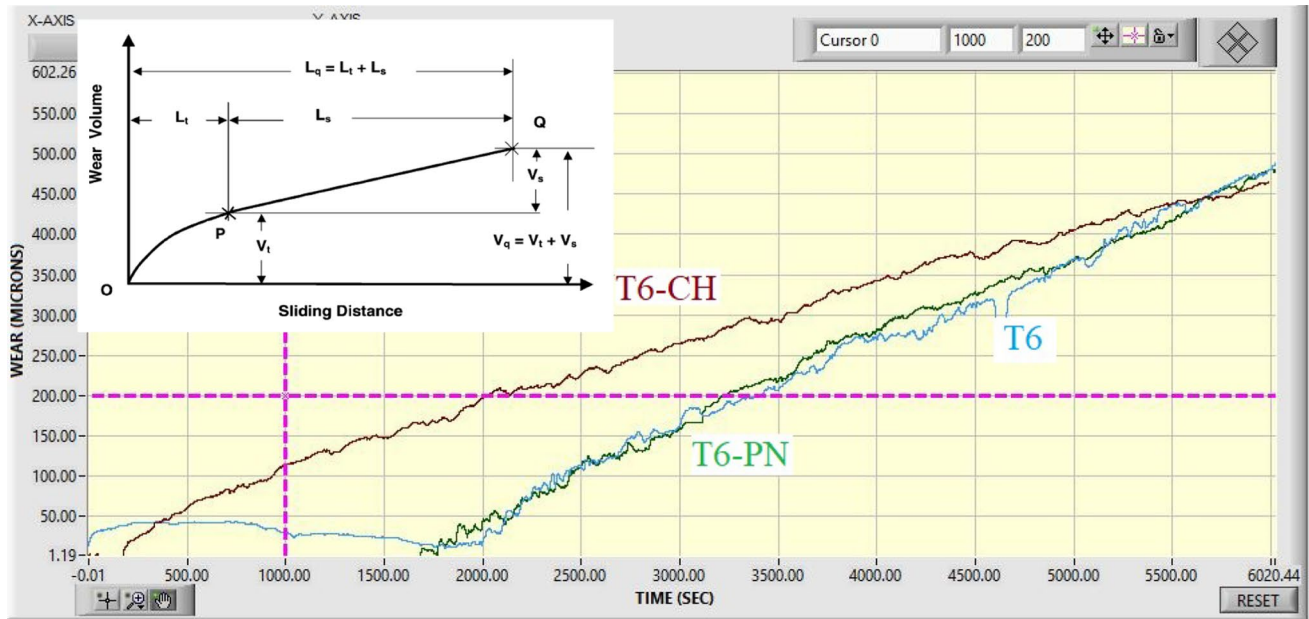
Fig. 6 Wear rate recorded for AAMMC for continues wear testing mode with schematic of wear model proposed

Table 4 PoD test at 450 °C: values of friction coefficient calculated in the steady-state (μ_{SS}) and the specific wear coefficient of composites (K_C)

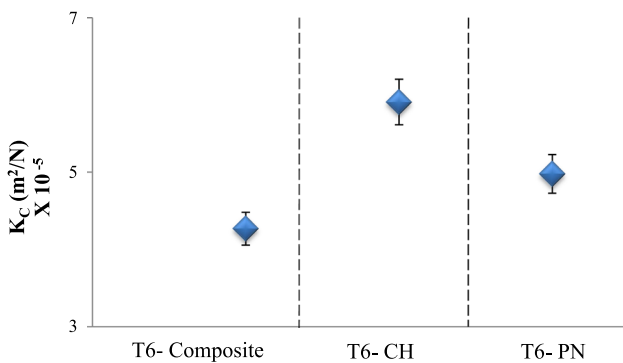| Composite tested for landing Distance 30,000 (m)	PoD dry sliding method Average ΔV (mm^3)	COF steady state (μ_{SS})	Specific wear coefficient K_C ($\times 10^{-5}$) [m^2/N]
T6	22.05	0.355 ± 0.02	4.27
T6-CH	17.29	0.372 ± 0.01	5.91
T6-PN	20.22	0.358 ± 0.02	4.98

Fig. 7 (K_C) Mean specific wear coefficient of the composite calculated for the PoD tests at 450 °C. Specimens of T6-composite, T6-CH, and T6-P

that T6-composite exhibited good wear performance which can be attributed to the homogenous nucleation of the precipitate on the surface. As microwave-assisted heat treating is performed on composites, most of the Al_2Cu solutes start to nucleate at matrix-α-Al_2O_3 interface and results in homogenous precipitation. After microwave-assisted heat treatment, T6-composite samples exhibit grain boundary precipitation, and encapsulation of α-Al_2O_3 particles which is in good agreement with the earlier sintering mechanics [22], and resulted in minimum particle pull out from the surface even after tested with extreme conditions (i.e. 100 N at 450 °C). No severe surface seizure and deep grooves or ploughing mechanism of the added α-Al_2O_3 particles are noticed in continuous wear mode.

On the T6-composite wear surface, the self-adhesive wear mechanism is observed, as a result of which the composite surface is spotted with plastic deformations containing Al_2Cu-α-Al_2O_3clusters. The formation of the cluster was observed in the direction opposite to the sliding direction. No proof of abrasive wear was observed on the composite surface. Very few fragmentation of the debris particles (III) is observed on the surface after the continuous wear testing. As the entire process was carried out at 450 °C, the self-adhesion observed on the surface was the material flow which is indicated by arrow heads in Fig. 8. In case of T6-PN specimen the wear mechanism is very similar as the
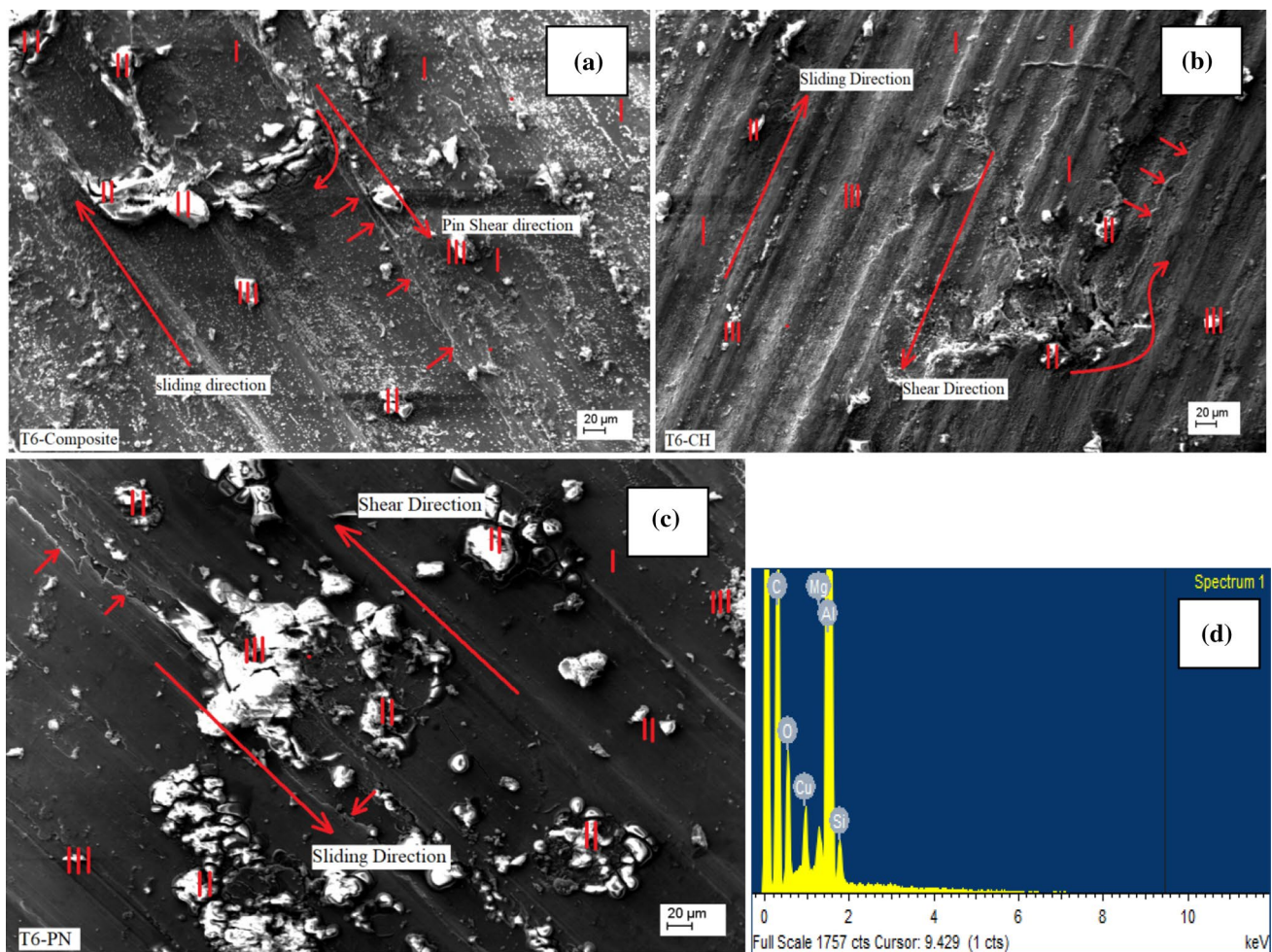
Fig. 8 Surface view of the worn composite after the PoD test for continuous wear at 450 °C. Specimens show the sliding direction, specimen shear directions, **a** T6 composites; **b** T6-CH composites; **c** T6-PN composites displaying (I) aluminium matrix, (II) α-Al$_2$O$_3$- Al$_2$Cu-matrix interface and (III) free debris and **d** EDX confirming the presence of Al$_4$C$_3$ phase formed at the α-Al$_2$O$_3$-Al$_2$Cu-matrix interface for T6-CH samples in Fig. 8c

T6-composite samples due to the complete absence of AlN layer. The resistance of the AlN layer on the T6-PN composite surface held the surface up to 2100 s of continuous wear which is evident from Fig. 6.

T6-CH composite after continuous wear at 450 °C exhibited a few traces of abrasive wear in the shearing direction as shown in Fig. 8. The spots marked as II in Fig. 8 (b) indicate that they are nucleated with the Al$_4$C$_3$ precipitates which act as a third body abrasive agent during the process which is confirmed by the EDX data provided in Fig. 8 (d) which clearly displays the carbon peaks which indicate the nucleated Al$_4$C$_3$ at the α-Al$_2$O$_3$-Al$_2$Cu-matrix interface. Composite surface during the process creates a plastic flow of matrix material (I) when obstructed by the projected surface asperities such as α-Al$_2$O$_3$-Al$_2$Cu particles which are indicated by arrows. This plastic flow of materials created plateaus of additional material that gets firmly welded to the

surface. This particular mechanism is specifically noticed in the T6-CH samples, and very few spots in T6-PN specimens are shown in Fig. 8. Very few micro-grooves because of ploughing action of the pulled out α-Al$_2$O$_3$ along with Al$_4$C$_3$ were noticed on the T6-CH samples as seen in Fig. 8.

Table 5 summarizes the compositional results of the EDX analyses performed on the composite worn surface and counter disc part to understand the material flow (I) during the process and the elements present on the composite surface after the continuous wear process. The major element is aluminium in all the composite samples which is present only in the pin. The elements present on the worn surface are majorly Al$_2$O$_3$ and carbide form of aluminium. In the samples of T6-CH, carbon element is found in excess on the surface because of microwave-assisted case hardening process as discussed earlier. Looking at the EDX data for the counter disc, it is evident that

Table 5 EDX validations on the worn composite surface and the counter disc part tested for continuous wear at 450 °C. Concentrations in wt%

Element	Weight%			Weight %		
	composite Pin			Counter Disc Part		
	T6-composite	T6-CH	T6-PN	Track tested for T6	Track tested for T6-CH	Track tested for T6-PN
Mg	1.2	1.4	1.2	0.3	0.2	0.3
Al	82.6	62.3	80.1	2.1	2.3	2.5
C	0.1	22.3	0.1	3.6	3.1	3.3
Si	0.6	0.5	0.5	2.3	2.7	2.3
O	11.4	10.2	11.5	2.5	2.9	2.6
Sn	0.6	0.7	0.7	0.7	0.6	0.6
Fe	0.1	0.1	0.1	87.8	87.6	84.9
Cu	3.4	2.5	3.2	0.2	0.1	0.5
N	–	–	2.6	–	–	2.6
Mn	–	–	–	0.5	0.5	0.4

pin materials when post-processed had very few impact in changing the surface element composition of the counterpart. Concentration of the other elements on the track of the counterpart was mainly because of the material getting alloyed or cold welded to the surface during the process. This phenomenon is mainly supported by the temperature at which the wear test was performed. Very few traces of aluminium is found on the track of the counter disc part after the continuous wear test as seen in Table 5. Particular attention was considerably paid to the presence of Sn content on the tracks of the process as shown in Table 5. The counter disc part had no trace of Sn before the process and recorded an average of 0.6–0.7 wt% of Sn. Another particular material to look for is the presence of nitrides on the wear tracks. N was recorded around 2.6 wt% which is mainly due to the presence of microparticles that settle down after the process on the wear tracks of the disc.

Figure 9 presents the HRSEM micrographs of the T6, T6-CH and T6-PN samples tested for short duration (time consumed for each landing scenarios experienced in aircraft landing). Composite surface is released to stop the rotating disc in the PoD setup acted upon with 4 MPa of pressure. It is evident from the HRSEM micrograph that no active wear mechanisms were observed on the surface of the composite irrespective of the sample type. However, T6-CH specimens were observed with very few surface seizures wear due to the surface roughness values after the microwave-assisted case hardening process. The surface seizures are marked with III in Fig. 9 which includes free microparticle debris formed during the testing for stopping distance. Minor fraction of plastic material flow was observed creating plateaus in T6-CH specimen tested for stopping distance. T6 and T6-PN samples had no trace of plateaus or surface seizure. T6-PN specimens left with no trace of wear debris after the process as shown in Fig. 9.

4 Discussion

In the current research work, the role of microwave-assisted case hardening and plasma nitriding on the microwave T6-treated composite for the dry sliding wear behaviour was investigated by adapting actual braking in a PoD setup. Aluminium alloy composite (reinforced with α-Al_2O_3) subjected to surface modification process has potentially improved the surface properties like reduced wear (μm) and regulated COF. The same trend was observed with respect to the specific wear coefficient of the composite (K_C): T6-CH samples displayed higher values compared to T6 and T6-PN samples. T6-CH samples had additional Al_4C_3 carbide form of aluminium which influenced the increase in K_{COF} the composite. However, combination of T6-CH (i.e. formation of Al_2Cu and Al_4C_3 on the surface) on the composite eventually improved the wear and COF characteristics. For the better understanding, a graph relating the COF and wear rate represented by K_C for the composite is displayed in Fig. 10. A second-order polynomial equation fits the obtained experimental data adequately. The significant fitting values are tabulated in Table 6.

This particular trend can be understood by studying the surface modification or altering the surface chemistry and surface properties of the composite which influences the tribological performance. This can be attributed to the additionally formed precipitates on the surface which acts as a resistant factor during the sliding wear [9, 25]. Necessary friction is generated between the composite pin and the rotating disc because of adhesive and abrasive mechanisms. The composite pin hardness is comparatively lower than that of the grey cast iron disc. Existing brake pad materials consist of various friction inhibiting constituents
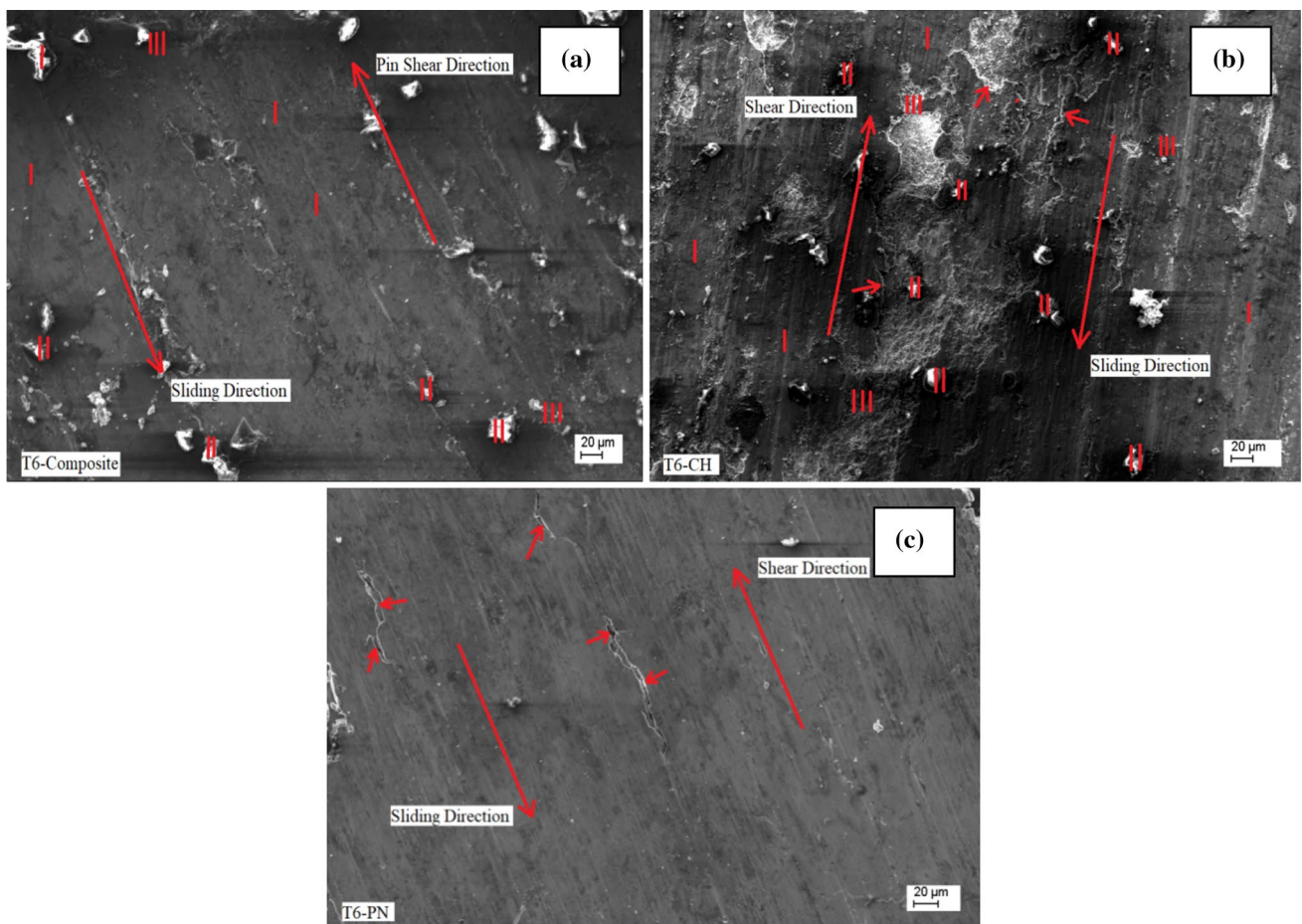
Fig. 9 Surface view of the worn composite after the PoD tests for stopping distance wear at 450 °C. Specimens show the sliding direction, specimen shear directions, **a** T6 composites **b** T6-CH composites and **c** T6-PN composites displaying (I) aluminium matrix, (II) α-Al$_2$O$_3$-Al$_2$Cu-matrix interface and (III) free debris
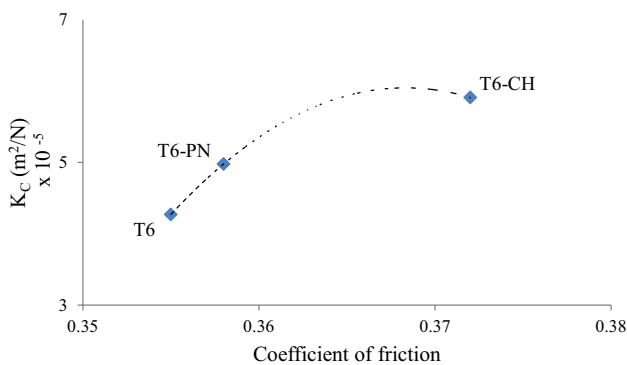

Fig. 10 Relation between the COF and the specific wear coefficient (K_C) for the composite: T6, T6-CH and T6-PN

Table 6 Parameters of the equation $(y = a + bx + cx^2)$ used to fit the experimental data in Fig. 10

a	b	C	Adj. R-Square
$7.37 * 10^{-4}$	$1.31 * 10^{-3}$	$-1.35 * 10^{-3}$	0.97

to improve the brake pad performance. In this current research work, aluminium alloy matrix is reinforced with 6 wt% α-Al$_2$O$_3$, followed by microwave-assisted T6-heat treatment and finally surface processed separately with microwave-assisted case hardening and plasma nitriding process. Accordingly, the developed composite is transformed into a potential friction material for brake pad application by enabling the ingredients to form the intermetallic compounds on the surface and near subsurface. Formation of Al$_2$Cu and Al$_4$C$_3$ precipitates on the surface and near subsurface improves the surface properties in terms of hardness and tribological aspects [26, 27].

Composite samples that are processed with plasma nitriding process developed a surface protecting layer of AlN with a thickness 40 μm which displayed a significant wear resistant medium in both the continuous wear mode and stopping distance mode. AlN layer formation

and bonding to the composite were fairly achieved because of the microwave processing on the composite [28]. Tin (Sn) as one of the alloying elements in AA 2900 facilitated in stabilizing the wear rate and the COF of the processed composites [29]. Composite during the microwave processing ended up displaying homogenous nucleation of the Al_2Cu and excellent sintering mechanism which created an excellent bonding strength between the matrix and reinforced α-Al_2O_3 [30]. These phenomena exhibited greater wear resistance at 450 °C and lesser K_C as shown in Fig. 10.

Figure 11 illustrates the evolution of the COF profiles, characteristically recorded for all the continuous wear mode of testing carried out with aircraft brake operation parameters in a PoD setup. In the continuous wear mode of testing at 450 °C, all the samples T6, T6-CH and T6-PN experienced a running period of 1000 s. It is observed that the COF reaches a steady state, determined by the type of processing method and presence of Al_2Cu, Al_4C_3 and α-Al_2O_3 and the alloying elements such as copper and Sn [29].

In continuous wear mode, the COF is characterized by a particular behaviour which is mainly influenced by the type of processing that was followed. On this note, three main stages of mechanism can be identified related to the COF curves presented in Fig. 11.

(A) A micro-lubrication medium made of Sn, which is formed during the continuous wear testing at 450 °C, is already present on the composite pin's surface and near subsurface in the matrix as well before starting the test. This is because of the composite pin's surface temperature which is heated to 450 °C by the pin heating module. However, during the process of composite pin heating up, the composite pin surface has no contact with the counterpart; at the starting of the continuous wear a sort of short run-in takes place in all types of composites, namely T6, T6-CH and T6-PN. This condition prevails until a complete contact between the two contact surfaces is established. As the melting point of Sn is 231.9 °C, micro-seepage of Sn on to the mating
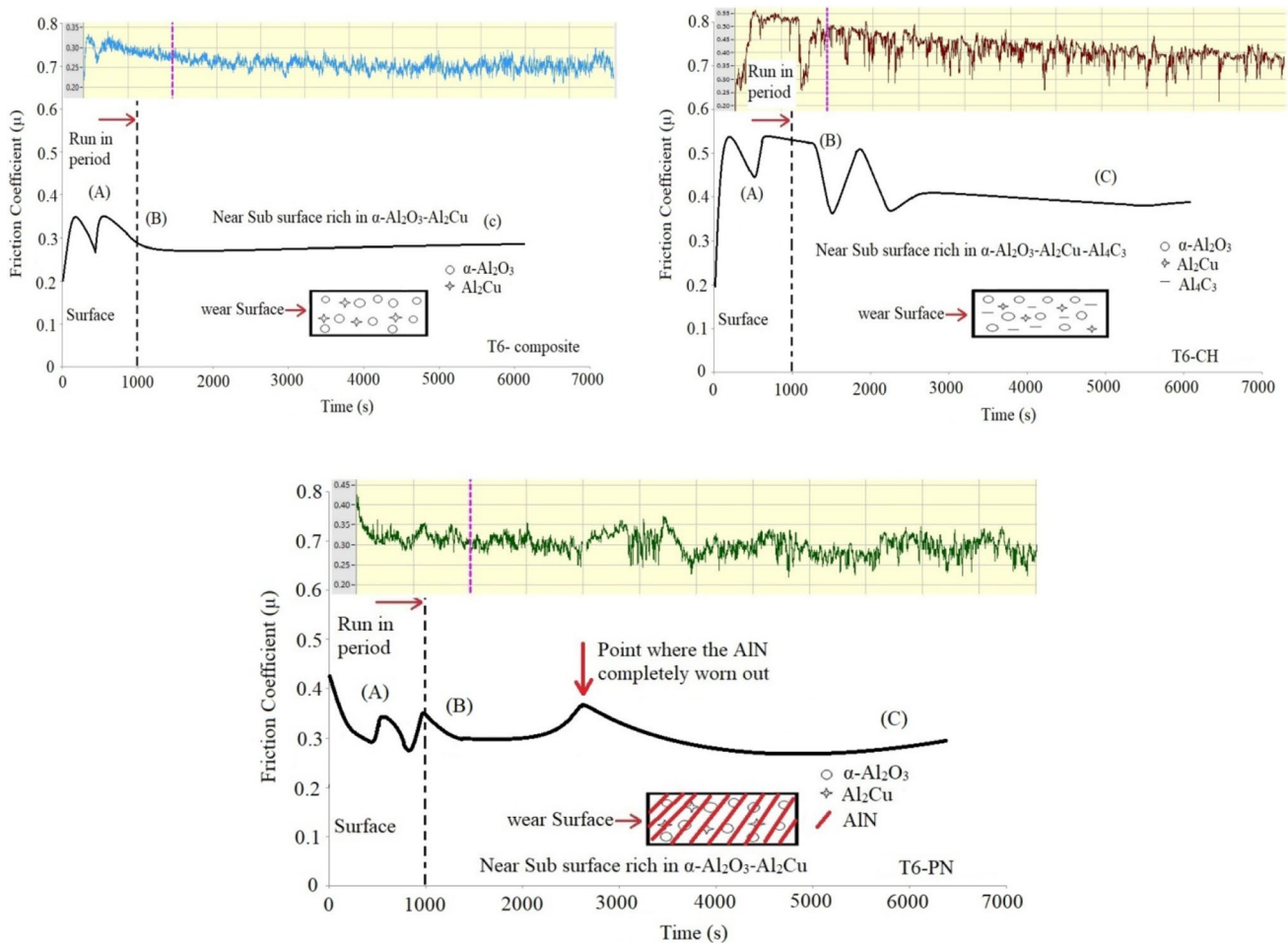

Fig. 11 Schematic illustration of the evolution of the COF for the continuous wear at 450 °C: T6, T6-CH and T6-PN. The plot describes the conditions of the surface of the composite specimen during continuous wear. See the main text for a full description

surfaces of the composite takes place which eventually leads to shorter run-in period in all types of composites and very early stabilization of the COF as seen in Fig. 11. Similar trend of Sn behaviour was reported by earlier investigations [29].

(B) The COF curve recorded a drastic declining trend in μ for T6-CH, due to the polishing effect that was achieved during the run-in period which tends the composite surface to lose its poor roughness layer that was noticed immediately after the microwave-assisted T6-CH process. Drastic decline in μ is also because of the micro-lubrication medium that is present at the friction surface of the composite pin heated at 450 °C. Especially in T6-CH samples, combined effects of Sn micro-lubrication at 450 °C, adhesion forces experienced at the contact surfaces and thermal softening of the composite pin surfaces are significant reason for the sudden decrease in μ. However, μ reaches a steady-state regime; this phenomenon is purely because of combined effect of alloying element Sn and microwave processing of the composite. Similar investigations reported elsewhere also have recorded the same trend of results and mechanisms [21, 27, and 29].

(C) In all the three types of composite (T6, T6-CH and T6-PN) samples the principal mechanism which exhibited a short run-in time, early steady-state achievement in the COF is microwave processing of the composite. In T6-CH samples, multiple particles like added α-Al_2O_3, Al_2Cu and Al_4C_3 are observed on the surface which creates a new raise in COF because of the slow wearing of the pin surface as shown in Fig. 8 and Fig. 11. T6 and T6-PN samples displayed a similar trend in the COF curve. This is mainly because of the presence of 40-μm-thick AlN layer, after which the T6-PN samples behaved similar to T6 samples. Once the AlN layer is completely worn out, the T6-PN samples are left to operate with added α-Al_2O_3 and formed Al_2Cu in the matrix. Above all, the early steady state was noticed in all types of composite because of the microwave-assisted T6 and microwave-assisted case hardening on the T6 sample.

The importance of the microwave processing had a significant impact on all the samples tested at 450 °C for continuous wear and stopping distance wear. Above all, T6-CH samples exhibited few COF peaks even after the short run-in period compared to T6 and T6-PN samples. It can be concluded that alloying element Sn, microwave-assisted processing on AA 2900–6 wt% α-Al_2O_3 significantly influenced the composite behaviour at aircraft brake test conditions. It is the role of micro-lubricant and friction coefficient stabilizer that perfectly happened at maximum brake operating temperature of 450 °C which is achieved by microwave processing. As microwave processing of composite is something which is heating from the core, heating by absorbing microwave and the novel sintering mechanism create a good interface bonding. During T6-heat treatment, the precipitates (Al_2Cu) are mostly formed on the reinforcement-matrix interface which created an encapsulation of the added α-Al_2O_3. During T6- microwave case hardening the homogenous nucleation of the diffused carbon into Al_4C_3 again happened at the reinforcement-matrix interface and at sometimes in reinforcement-matrix-precipitate interface [10]. Because of this mechanism the reinforcement and other precipitate constituents formed on the surface and near subsurface during the process were not quickly removed as worn debris [22], and indeed all the microwave processed composite samples show a drastic decrease in the composite specific wear coefficient (K_C).

T6-PN samples experienced two steady-state COF regimes: one before losing the AlN layer and the other after losing AlN layer as shown in Fig. 11. In the first regime, the AlN was seen with very little Sn micro-lubrication medium on the contact surface because of which the T6-PN samples experienced a slight higher COF as shown in Fig. 11. Once the surface of the samples is completely worn out of AlN, a sudden peak in COF was observed as shown by an arrow mark in Fig. 11. The composite surface and the AlN layer interface experienced a surplus of Sn medium which made the AlN to completely worn out from the surface. During the process, AlN conducts the contact interface temperature through the layer and dissipates onto the composite body. This phenomenon creates an additional thermal energy to form a discrete micro-lubricating medium between the AlN and composite surface interface. This kind of mechanism weakens the AlN layer, and it got completely worn out at 2100s where its purpose of protecting the surface is jeopardized at 450 °C. After the complete worn out of AlN from the contact interface in the form of wear debris, traces are seen on the wear track as shown in EDX results tabulated in Table 5. In the second regime of steady-state COF, T6-PN samples exhibited the similar steady-state behaviour of COF experienced in T6 composites as shown in Fig. 11.

5 Conclusions

The effect of the microwave-assisted case hardening and plasma nitriding on the microwave T6-AA2900-α-Al_2O_3 composite was investigated for actual aircraft braking conditions using a PoD test machine. The study considered the tribological performance of the newly surface processed aluminium composites against a grey cast iron as priority requirement. The significant findings can be summarized as follows:

- AA2900 with the discrete alloying elements such as Sn impacts considerably on the specific wear coefficients K_C and the COF of the composites.
- In the continuous and stopping distance wear at maximum aircraft brake operating temperature (i.e. 450 °C), microwave processed composite samples exhibited excellent tribological performance close to the existing brake pad material.
- The near preeminent tribological performance was noticed in the T6-PN samples which had COF closer to actual brake performance expectations with satisfactory specific wear coefficient K_C regimes. T6 and T6-CH samples exhibited lesser and higher K_C respectively. But T6-CH samples exhibited good wear performance which was recorded to be closest to the T6-PN samples.
- T6-PN samples with AlN layer on the surface remained as a strong protective layer till 2100s of continuous wear.
- Microwave processing emerged as a proven method to convert aluminium composite as a potential material which can be considered for the aircraft brake friction application.
- The material without surface modification exhibited lesser tribological performance compared to T6-CH and T6-PN with respect to K_C and COF.

References

1. Brake Friction Material - Restrictions on Use, Substitute Senate Bill 6557, 2010.
2. Kumar, M.; Bijwe, J.: Non-asbestos organic (NAO) friction composites: role of copper; its shape and amount. Wear 270, 269–280 (2011). https://doi.org/10.1016/j.wear.2010.10.068
3. Barros, L.Y.; Poletto, J.C.; Neis, P.D.; Ferreira, N.F.; Pereira, C.H.S.: Influence of copper on automotive brake performance. Wear 426, 741–749 (2019).
4. Filip, P.; Kovarik, L.; Wright, M.A.: Automotive brake lining characterization. SAE Tech. Pap. Ser. (2010). https://doi.org/10.4271/973024
5. Chan, D.; Stachowiak, G.W.: Review of automotive brake friction material. Proc. Inst. Mech. Eng. - Part D J. Automob. Eng. 218, 953–966 (2004). https://doi.org/10.1243/0954407041856773
6. Eriksson, M.; Bergman, F.; Jacobson, S.: On the nature of tribological contact in automotive brakes. Wear 252, 26–36 (2002). https://doi.org/10.1016/S0043-1648(01)00849-3
7. Osterle, W.; Deutsch, C.; Gradt, T.; Orts-Gil, G.; Schneider, T.; Dmitriev, A.I.: Tribological screening tests for the selection of raw materials for automotive brake pad formulations. Tribol. Int. 73, 148–155 (2014). https://doi.org/10.1016/j.triboint.2014.01.017
8. Rohatgi PK. 9th edCast metal matrix composites, metal hand book, Vol 15. ASM International; 1988.
9. Wang, A.; Rack, H.J.: Transition wear behaviour of SiC-particulate and SiC- whisker-reinforced 7091 Al metal matrix composites. Mater. Sci. Eng. A147, 211–224 (1991)
10. Pan, Y.M.; Fine, M.E.; Gheng, H.S.: Aging effects on the wear behaviour of P/M aluminu alloy SiC particle composite. ScrMetall 24, 1341–1345 (1990)
11. Pan, Y.M.; Fine, M.E.; Gheng, H.S.: Sliding wear of an alloy SiC whisker composite. Tribol Trans 35, 482–490 (1992)
12. Ma, B.; Wang, J.; Lee, T.H.; Dorris, S.E.; Wen, J.; Balachandran, U.: Microstructural characterization of Al_4C_3 in aluminum–graphite composite prepared by electron-beam melting. J. Mater. Sci. 53, 10173–10180 (2018)
13. Chan, D.S.E.A.; Stachowiak, G.W.: Review of automotive brake friction materials. Proc. Inst. Mech. Eng., Part D: J. Automob. Eng. 218, 953–966 (2004)
14. Telang, A.K.; Rehman, A.; Dixit, G.; Das, S.: Alternate materials in automobile brake disc applications with emphasis on Al composites–a technical review. J. Eng. Res. Stud. 1, 35–46 (2010)
15. Tan, C.; Kuang, T.; Zhou, K.; Zhu, H.; Deng, Y.; Li, X.; Cai, P.; Liu, Z.: Fabrication andcharacterization of in-situ duplex plasma-treated nanocrystalline Ti/AlTiNcoatings. Ceram. Int. 42, 10793–10800 (2016)
16. Enes, A.; Ali, G.; Gökhan, Y.: Effects of cooling rate on strength and microstructure of powder metallurgy superalloys. Period. Eng. Nat. Sci. 5, 15–27 (2017)
17. Gadow, R.; Jiménez, M.: Carbon fiber-reinforced carbon composites for aircraft brakes. Am. Ceram. Soc. Bull. 98, 28–34 (2019)
18. Hiremath, A.: A study to evaluate the effect of carburization on LM13 aluminium alloy–quartz composites anupama A. Int. J. Eng. and Technol. (UAE) 7, 145–149 (2018)
19. Sahin, Y.; Kilicli, V.: Abrasive wear behaviour of SiCp/Al alloy composite in comparison with ausferritic ductile iron. Wear 271(11–12), 2766–2774 (2011)
20. Miyajima, T.; Iwai, Y.: Effects of reinforcements on sliding wear behavior of aluminum matrix composites. Wear 255(1–6), 606–616 (2003)
21. Ashwath, P.; Joel, J.; Jeyapandiarajan, P.; Xavior, A.; Rajendran, R.: Frictional property evaluation of aluminium alloy based metal matrix composites under dry braking condition in pin—on—disc system. Mater. Res. Expr. 7(1), 016509 (2019)
22. Ashwath, P.; Anthony Xavior, M.: Effect of microwave heat treating processing on frictional behaviour of aluminium alloy 2900 composites. Tribol-Mater., Surf. Interf. 12(2), 85–96 (2018)
23. Yang, L.J.: Wear coefficient equation for aluminium-based matrix composites against steel disc. Wear 255(1–6), 579–592 (2003)
24. Yang, L.J.: A methodology for the prediction of standard steady-state wear coefficient in an aluminium-based matrix composite reinforced with alumina particles. J. Mater. Process. Technol. 162, 139–148 (2005)
25. Dileep, B.P.; Vitala, H.R.; Megalingam, A.; Karthik, K.: Mechanical and tribological characterization nitrided Al-7075/Al2O3 metal matrix composites. Period. Eng. Nat. Sci. 6(2), 64–70 (2018)
26. Darsono, Febri Budi, TeguhTriyono, and EkoSurojo. "The effect of case hardening treatment on aluminum 7075 toward its hardness and tensile strength." In AIP Conference Proceedings, vol. 1931, no. 1, p. 030058. AIP Publishing LLC, 2018.
27. Guo, B.; Chen, B.; Zhang, X.; Cen, Xi.; Wang, X.; Song, M.; Ni, S.; Yi, J.; Shen, T.; Yong, Du.: Exploring the size effects of Al_4C_3 on the mechanical properties and thermal behaviors of Al-based composites reinforced by SiC and carbon nanotubes. Carbon 135, 224–235 (2018)
28. Visuttipitukul, P.; Aizawa, T.; Kuwahara, H.: Feasibility of plasma nitriding for effective surface treatment of pure aluminum. Mater. Trans. 44(7), 1412–1418 (2003)
29. Bishop, D.P.; Li, X.Y.; Tandon, K.N.; Caley, W.F.: Dry sliding wear behaviour of aluminum alloy 2014 microalloyed with Sn and Ag. Wear 222(2), 84–92 (1998)
30. HülyaKaçar, D.; Meric, C.: Age-hardening behavior of powder metallurgy AA2014 alloy. Mater Des 28(3), 982–986 (2007)